Sea surface slope statistics derived from Sun glint radiance measurements and their apparent dependence on sensor elevation

Vincent Ross[1] and Denis Dion[2]

Received 1 February 2007; revised 17 May 2007; accepted 4 June 2007; published 20 September 2007.

[1] Sea surface slope variances are obtained by inverting narrowband (444, 501, 677, and 864 nm) Sun glint radiance measurements using a detailed analytical specular sea surface bidirectional reflectance distribution function (BRDF) that includes mutual wave shadowing and hiding. The resulting data set spans a wide range of environmental conditions including wind speeds from 0.5 to 13.5 m s^{-1} and many different viewing and source geometries. Analysis against wind speed and atmospheric stability produces trends similar to those found in previous studies, as well as finer tendencies that were formerly difficult to detect. Furthermore, the detailed nature of the BRDF model used in the analysis permits an investigation of the correlation of the statistics with viewing geometry, revealing a strong relationship between sensor elevation and measured slope variance, especially at grazing angles.

Citation: Ross, V., and D. Dion (2007), Sea surface slope statistics derived from Sun glint radiance measurements and their apparent dependence on sensor elevation, *J. Geophys. Res.*, *112*, C09015, doi:10.1029/2007JC004137.

1. Introduction

1.1. Overview

[2] Accurate modeling of the roughness of the sea, particularly of the sea slope statistics, has many beneficial implications in remote sensing and radiation budget studies. Most interactions of radiation with the air-sea boundary depend on the roughness of the interface, which makes it a key factor when modeling the bidirectional reflectance distribution function (BRDF) of the sea surface. Our knowledge of the radiative properties of the surface will undeniably affect the understanding of remote measurements of any quantity at or across the air-sea interface. Consequently, many efforts have been spent on the creation of various types of sea BRDF models. Some involve analytical approximations [*Mermelstein et al.*, 1994; *Zeisse*, 1994, 1995], while others are based on complex 3D Monte-Carlo surface modeling [*Preisendorfer and Mobley*, 1986; *Bourlier et al.*, 2000a, 2000b; *Henderson et al.*, 2003]. No matter how complex or realistic models may be, most are firmly based on an understanding of the sea surface slope or wave statistics. This implies that no sea BRDF model will ever be more accurate than its underlying description of the sea surface. It is therefore of prime importance to have the option of using a model that describes the statistical properties of the sea surface under varying environmental conditions with as much accuracy as possible.

[3] One method to obtain a description of the sea surface statistics is to derive sea slope variances from a wave power density spectrum according to

$$\alpha = \frac{1}{2}\int_0^\infty k^2 \mathrm{S}(k)dk, \qquad \beta = \frac{1}{4}\int_0^\infty k^2 \mathrm{S}(k)\Delta(k)dk \tag{1}$$

where k is the wave number, $S(k)$ is the omnidirectional spectrum, and $\Delta(k)$ is the upwind-crosswind ratio term in the angular spreading function which describes the variations of the spectrum according to wave number and direction (usually in reference to the wind direction). From equation (1), the upwind and crosswind slope variances are then obtained with

$$\sigma_x^2 = \alpha + \beta, \quad \sigma_y^2 = \alpha - \beta. \tag{2}$$

[4] Theoretical and empirical wave spectra have been in development for many decades. Much of the early work [e.g., *Phillips*, 1958; *Toba*, 1973; *Hasselmann et al.*, 1973; *Phillips*, 1985] concentrated mostly on the longer wavelength gravity waves, mainly because of the lack of measurements and theoretical understanding of the short gravity and capillary wave regions of the spectrum. Since short waves contribute significantly to slope statistics, these spectra usually fail to reproduce field slope measurements. Later on, in part because of the advent of microwave remote sensing, investigators like *Donelan and Pierson* [1987] and *Apel* [1994] attempted to incorporate up-to-date field measurements and theoretical considerations into the gravity-

[1]AEREX Avionique Inc., Breakeyville, Quebec, Canada.
[2]Defence Research and Development Canada-Valcartier, Quebec, Quebec, Canada.

capillary wave region. Although these spectra were, and are still in wide use for microwave remote sensing, they again fail to produce wave slope statistics in accordance with optical measurements [*Elfouhaily et al.*, 1997; *Liu et al.*, 2000; *Ross and Dion*, 2004]. More recently, researchers like *Elfouhaily et al.* [1997], *Liu et al.* [2000] and *Hwang* [2005] have again bettered the intermediate to capillary spectral region of existing models. These new formulations seem to agree quite well with the available optical field measurements of slope statistic, but since these are not numerous and have a high degree of scatter, accurate validation is difficult. The relative lack of published results is mostly due to the experimental difficulties involved. One can attempt to reproduce natural conditions in a laboratory, but experience has shown that wave tank measurements do not always reproduce field measurements correctly [*Shemdin and Hwang*, 1988; *Wu*, 1990]. Since a great number of environmental factors seem to influence sea surface statistics, more in situ data are required to better verify the many correlations.

[5] The objective of this paper is to add to the existing data sets and to propose a mean to facilitate sea surface slope statistical studies in the future. To do this, a newly developed detailed specular sea BRDF model is inverted to extract slope probability density values from Sun glint radiance measurements under varying meteorological conditions. Slope probability density functions (PDF) are then fitted to the extracted values and analyzed against environmental and geometrical conditions.

1.2. Slope Variance Models

[6] The first reliable set of sea slope statistical measurements was obtained by *Cox and Munk* [1954a, 1954b] from photographs of Sun glint. The photographs were taken from an airplane at about 600 m in altitude while meteorological data was gathered from a ship down below. Care was taken for the Sun to be high enough so that the effects of shadowing and multiple reflections were small. They found that the PDF was well fitted by a Gram-Charlier expansion whose first-order term is the Gaussian

$$p_0(\zeta_x, \zeta_y|U) = \frac{1}{2\pi\sigma_x\sigma_y}\exp\left\{-\frac{1}{2}\left(\frac{\zeta_x^2}{\sigma_x^2}+\frac{\zeta_y^2}{\sigma_y^2}\right)\right\} \tag{3}$$

where U is the wind speed at 12.5 m, ζ_x and ζ_y are the upwind and cross wind slopes, and σ_x and σ_y are the upwind and crosswind variances. They also found a linear relationship between variances and wind speed

$$\begin{aligned}\sigma_x^2 &= 0.00316U \pm 0.004\\ \sigma_y^2 &= 0.003 + 0.00192U \pm 0.004.\end{aligned} \tag{4}$$

Additional terms are needed to correct for kurtosis (peakedness) and skewness,

$$\begin{aligned}p \approx p_0\Big\{1 &- \frac{1}{2}c_{21}(Y^2-1)X - \frac{1}{6}c_{03}(X^3-3X)\\ &+ \frac{1}{24}c_{40}(Y^4-6Y^2+3) + \frac{1}{4}c_{22}(Y^2-1)(X^2-1)\\ &+ \frac{1}{24}c_{04}(X^4-6X^2+3)\Big\},\end{aligned} \tag{5}$$

where

$$X = \frac{\zeta_x}{\sigma_x}, \quad Y = \frac{\zeta_y}{\sigma_y}.$$

The *Cox and Munk* [1954a, 1954b] skewness expansion coefficients in equation (5) are given by

$$c_{21} = 0.01 - 0.0086U, \quad c_{03} = 0.04 - 0.033U \tag{6}$$

while the kurtosis coefficients are

$$c_{40} = 0.40, \quad c_{22} = 0.12, \quad c_{04} = 0.23. \tag{7}$$

Although the Gram-Charlier series representation of the sea slope PDF has rarely been disputed in the literature (*Liu et al.* [1997] and *Plant* [2003] are a few exceptions), some improvements or alternatives to the slope variance model (4) have been proposed. Two decades after Cox and Munk, *Wu* [1972] reanalyzed their data to notice that a two-branch logarithmic function could yield a better fit. *Wu* [1990] later revised his relationship and finally obtained a new relationship between sea slope variances and wind speed given by

$$\begin{aligned}\sigma^2 &= (0.90 + 1.20\ln U_{10})\times 10^{-2} \;\; U_{10} \le 7\ \text{m/s}\\ \sigma^2 &= (-8.40 + 6.00\ln U_{10})\times 10^{-2} \;\; U_{10} > 7\ \text{m/s}\end{aligned} \tag{8}$$

where U_{10} is the wind speed measured at 10 m and σ^2 is the average upwind and crosswind variance ($[\sigma_x^2 + \sigma_y^2]/2$). The upwind and crosswind components are obtained from the constant relation $\sigma_y^2/\sigma_x^2 = 0.8$. According to Wu, the two branches of the equation correspond to gravity-dominant and capillary-dominant wave regimes, respectively.

[7] Subsequently, the advent of the laser has prompted a few other sea slope measurement campaigns [*Hughes et al.*, 1977; *Tang and Shemdin*, 1983; *Haimbach and Wu*, 1985; *Hwang and Shemdin*, 1988; *Shaw and Churnside*, 1997]. Most of the time, results obtained have been in accord with those obtained by Cox and Munk, but occasionally, major deviations were observed. Authors have attempted to correlate these deviations with other environmental parameters such as atmospheric stability or swell conditions. *Hwang and Shemdin* [1988] found that although the state of development of swells had some influence, it was small compared to the effect of atmospheric stability. This was later confirmed by *Shaw and Churnside* [1997], who added their data to that of Hwang and Shemdin and obtained an expression modifying *Cox and Munk*'s [1954a, 1954b] variances to take into account atmospheric stability.

[8] As mentioned in the previous section, apart from expressions derived from the original work of Cox and Munk, the only other available relationships are those derived from wave power density spectra. Among the spectra that seem to translate well to slope variance values, the *Elfouhaily et al.* [1997] spectrum was specifically developed on the basis of the criteria that it should reproduce the optical slope variance data of *Cox and Munk* [1954a, 1954b], as well as describe the dynamics of gravity-capillary wave curvature measures by *Jähne and Riemer* [1990] (laboratory measurements) and *Hara et al.*

[1994] (field measurements). It was also designed to easily adjust to future measurements as they become available. Furthermore, the spectrum is related to important physical quantities such as wind fetch and atmospheric stability. This model is thus used in this study to demonstrate how large amounts of slope variance data can give insight into the validity of certain features of a spectrum.

2. BRDF Model

[9] The bidirectional reflectance distribution function in its reciprocal and normalized form is usually described as the ratio of radiance L_r of the surface in the receiver direction $\mathbf{\Psi}_r = (\theta_r, \phi_r)$ and the source irradiance incident on the surface $E_s \cos\theta_s$ from source direction $\mathbf{\Psi}_s = (\theta_s, \phi_s)$

$$f(\mathbf{\Psi}_s, \mathbf{\Psi}_r) = \frac{\pi L_r(\mathbf{\Psi}_r)}{E_s(\mathbf{\Psi}_s)\cos\theta_s} \tag{9}$$

where θ_s is the angle between the source and the average surface normal (zenith angle for a horizontal surface) and ϕ denotes the azimuth angles. A statistical specular BRDF model is always proportional to the probability that the geometrical configuration, or slope vector $\boldsymbol{\zeta} = (\zeta_x, \zeta_y)$ of the surface, can produce a specular reflection from the source to the receiver

$$f(\mathbf{\Psi}_s, \mathbf{\Psi}_r) \propto p(\boldsymbol{\zeta}) \tag{10}$$

where p is called the occurrence PDF. Knowing the source irradiance at the surface, it is then possible to obtain a value of the slope PDF from measurements of the average specular reflected radiance. Doing this for many receiver and source geometries then yields the overall PDF, or at least a good portion of it. This is the method used originally by *Cox and Munk* [1954a, 1954b] where they approximated the BRDF to be essentially equal to the product of the occurrence PDF and the reflection geometry's Fresnel coefficient. When using such a simplistic approximation, one has to be aware of limitations arising from shadowing, and to a smaller degree, from multiple reflection effects that arise mainly at shallower reflection angles. For these reasons either a substantial amount of potentially valuable data must be discarded, or complex and expensive experimental setups must be devised to carry out near nadir measurements (from an airplane, for example). It is therefore desirable to use a BRDF model that includes these effects as much as possible. Until recently, detailed BRDF models did not have an analytical form from which the occurrence PDF could be extracted. A newly developed model applicable to a height-slope uncorrelated quasi-Gaussian surface [*Ross et al.*, 2005] now offers such a possibility. The BRDF can be expressed in the form of equation (9) as

$$f(\mathbf{\Psi}_s, \mathbf{\Psi}_r) = \frac{\pi r(\mathbf{\Psi}_s, \mathbf{\Psi}_r) q_{vn}(\mathbf{\Psi}_s, \mathbf{\Psi}_r)}{4 z_n^3 (\mathbf{U}_n \cdot \mathbf{U}_r)\cos\theta_s} \tag{11}$$

where q_{vn} is the normalized visible interaction PDF and is related to the occurrence PDF by

$$q_{vn}(\mathbf{\Psi}_s, \mathbf{\Psi}_r) = \frac{p(\boldsymbol{\zeta}) W(\boldsymbol{\zeta}, \mathbf{\Psi}_r) H_\zeta(\boldsymbol{\zeta}, \mathbf{\Psi}_r)}{[1 + \Lambda(v_r) + \Lambda(v_s)]\cos\theta_r} \tag{12}$$

with

$$W(\boldsymbol{\zeta}, \mathbf{\Psi}_r) = \frac{\mathbf{U}_n \cdot \mathbf{U}_r}{z_n} \tag{13}$$

which accounts for projection onto the receiver direction,

$$H_\zeta(\boldsymbol{\zeta}, \mathbf{\Psi}_r) = \Upsilon(\mathbf{U}_n \cdot \mathbf{U}_r) \tag{14}$$

which accounts for not seeing the backside of waves, where Υ is the Heaviside function, and where

$$\Lambda(v) = \frac{\exp(-v^2) - v\sqrt{\pi}\,\mathrm{erfc}(v)}{2v\sqrt{\pi}}, \quad v = \frac{\cot(\theta)}{\sqrt{2}\sigma(\phi)}.$$
$$\sigma(\phi) = \sqrt{\sigma_x^2 \cos^2\phi + \sigma_y^2 \sin^2\phi} \tag{15}$$

[10] Equation (15) applies to receiver ($\Lambda(v_r)$) or source ($\Lambda(v_s)$) elevation and is a result of the integration of the *Smith* [1967a, 1967b] height shadowing function. In these expressions $\mathbf{U}_n$ is the Cartesian surface facet normal unit vector, $\mathbf{U}_r$ is the surface to receiver unit vector, z_n is the zenith component of $\mathbf{U}_n$, and finally, $r(\mathbf{\Psi}_s, \mathbf{\Psi}_r)$ is the Fresnel reflection coefficient.

[11] Equating functions (9) and (11), and using equation (12), we obtain an expression for the occurrence PDF for a particular $\boldsymbol{\zeta}$ that is uniquely determined by geometry ($\mathbf{\Psi}_s$, $\mathbf{\Psi}_r$)

$$p(\boldsymbol{\zeta}) = \frac{4 z_n^3 (\mathbf{U}_n \cdot \mathbf{U}_r)[1 + \Lambda(v_r) + \Lambda(v_s)]\cos\theta_r L_r(\mathbf{\Psi}_r)}{r(\mathbf{\Psi}_s, \mathbf{\Psi}_r) W(\boldsymbol{\zeta}, \mathbf{\Psi}_r) H_\zeta(\boldsymbol{\zeta}, \mathbf{\Psi}_r) E_s(\mathbf{\Psi}_s)}. \tag{16}$$

Note that in this context $H_\zeta(\boldsymbol{\zeta}, \mathbf{\Psi}_r) = 1$ always holds since measuring the reflected radiance off a facet implies that it is visible from the receiver's point of view.

[12] Although this expression is applicable to a point source, it has been shown by *Ross et al.* [2005] that using the Sun's irradiance and center position produces an error smaller than 1% on the resulting observed reflected radiance for any slope variance as long as the Sun is more than 10° above the horizon. Equation (16) thus provides an efficient mean to easily obtain slope PDF values from measurements of Sun irradiance and its specular surface reflected radiance. Furthermore, it allows one to investigate receiver and source geometries not accessible before.

3. Measurements Analysis

[13] The measurements used in this study are publicly available from the Clouds and the Earth's Radiant Energy System (CERES) Ocean Validation Experiment (COVE). They are obtained from a rigid ocean platform located 25 km off the cost of Virginia Beach at the mouth of Chesapeake Bay. The instrument is a SP1A Schultz spectral photometer fixed 23 meters above sea level that scans the sea surface at

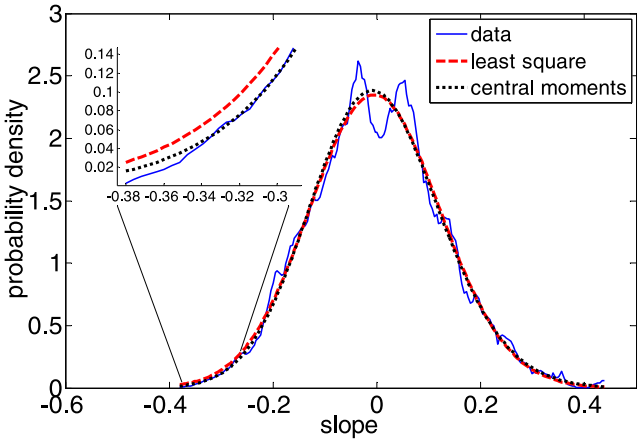

Figure 1. Typical example of integrated PDF data fitted with a Gram-Charlier distribution by methods of least squares and central moments, for a given wind speed bin.

10 elevation angles from 2° to 72° from the horizontal. For each elevation angles, it scans about 180° of azimuth at 2.5° intervals. For each new scan, narrowband filters are rotated among 444 nm, 501 nm, 677 nm and 864 nm. More information on the instrument and data are given by *Su et al.* [2002]. Note that the scanning resolution and spans have been modified slightly since their publication. Meteorological and environmental data for the COVE site are also readily available from the NASA Langley CERES Atmospheric Radiation Measurement (ARM) Validation Experiment (CAVE) [*Rutan et al.*, 2001; *Jin et al.*, 2002]. For this study, we used all measurements taken on cloudless periods in the months of August 2003 through February 2004. In all, data from 26 days are considered, encompassing wind speeds ranging from about 0.5 to 13.5 m s^{-1} and spanning a wide range of Sun receiver geometries. It is worth mentioning that wind speeds are measured at 38 meters and need to be scaled down to 10 meters in altitude using the Monin-Obukhov theory [*Monin and Obukhov*, 1954].

[14] In our analysis, we use equation (16) to relate the occurrence PDF to the specular component of the solar reflected radiance. Since only the solar contribution is considered, all parasitic radiance components must be subtracted as best possible from the data before it can be used. Parasitic components of the surface radiance in the concerned wavelength bands are mainly composed of sky reflections off the surface as well as subsurface scattering off sediment, organic matter, and water itself. Also to be removed are the atmospheric components of the radiance such as gas and aerosol scattering. Extinction of radiation by the atmosphere to varying degrees depending on viewing geometry must also be taken into account.

[15] An empirical method was used to remove the path-scattered atmospheric radiance and the sky reflections from the measurements. An empirical method is justified since trying to model the parasitic contributions would likely be error prone. We can take advantage of the fact that the slope PDF for the Sun's geometry quickly drops to negligible values at azimuths a few degrees off the Sun center, and that the parasitic component is a relatively smooth function of azimuth. This means we can easily eliminate data azimuths likely to contain Sun glint, and fit a parametric function to the remaining data. The fitted function is then subtracted from the overall data, leaving essentially the glint component. Because the sky reflected component should be close to a Gram-Charlier distribution (although highly convoluted), it was chosen as the fitting function. During this study, an attempt to subtract modeled parasitic radiance has shown the empirical method to be far superior, and that the Gram-Charlier distribution fits the parasitic component quite well. The only modeled parasitic component is the transmittance from the surface to the sensor. The transmittances are modeled using MODTRAN4 [*Berk et al.*, 1989; *Acharya et al.*, 1999] together with the LWKD [*Forand*, 1999], a surface layer aerodynamic model based on the Monin-Obukhov theory, and WKDAER [*Dion et al.*, 2004] (available by e-mailing the authors) for the calculation of marine aerosol extinction. Transmittance modeling is less sensitive to aerosol modeling errors than radiance, and at 2° from the horizontal, the corrections rarely exceed 15%, so the overall error on the corrected data should be only a small fraction of this.

[16] Once all data have been processed so that only the Sun glint component remains, equation (16) is applied to transform the Sun irradiance measured at the COVE site into occurrence PDF points. Shadowing (terms $\Lambda(v_r)$ and $\Lambda(v_s)$) is approximated using the *Cox and Munk* [1954a, 1954b] statistics. Fear that this could bias the results toward the *Cox and Munk* [1954a, 1954b] statistics should be put aside for many reasons. First of all, shadowing is not a major component of the BRDF. The combination of shadowing and multiple reflections should not account for more than 2 or 3 percent of the overall reflectance when the wind is blowing at 10 m s^{-1} and the Sun is 10° or more above the horizon [*Preisendorfer and Mobley*, 1986]. Furthermore, the shadowing functions are not nearly as sensitive to variations in slope variance as is the occurrence PDF, nor do they affect the width of the glint pattern (and thus variance) significantly. Should there be a bias, it would likely be much smaller than the measurement errors.

[17] For each date, the data are then binned by wind speed increments so that each bin contains between 10 000 and 20 000 PDF data points (depending on the measurements availability at a given wind speed). Such a great number of data points are necessary since the instrument takes almost instantaneous snapshots of the radiance in a 1° aperture, resulting in very noisy data. For each wind bin, points are interpolated to a fixed slope grid and integrated in both upwind and cross wind directions yielding the measured components of the PDF. Finally, a Gram-Charlier function is fitted to these components using two different methods. The first is a simple least squares fit while the second is done by computing the central moments of the distribution. Both methods usually yield slightly different variance values, but these differences are not systematic. On some rare occasions the central moment method may be less accurate if the slope range is not large enough. We thus consider the average of the results from the two methods weighed by the inverse of the regression variance (which favors the least square method) in order to reduce errors. A typical example of a fitted PDF is provided in Figure 1. We note that both methods yield similar results, although the central moments may better reproduce low slope values (better kurtosis) as seen in the magnified part of the curve.

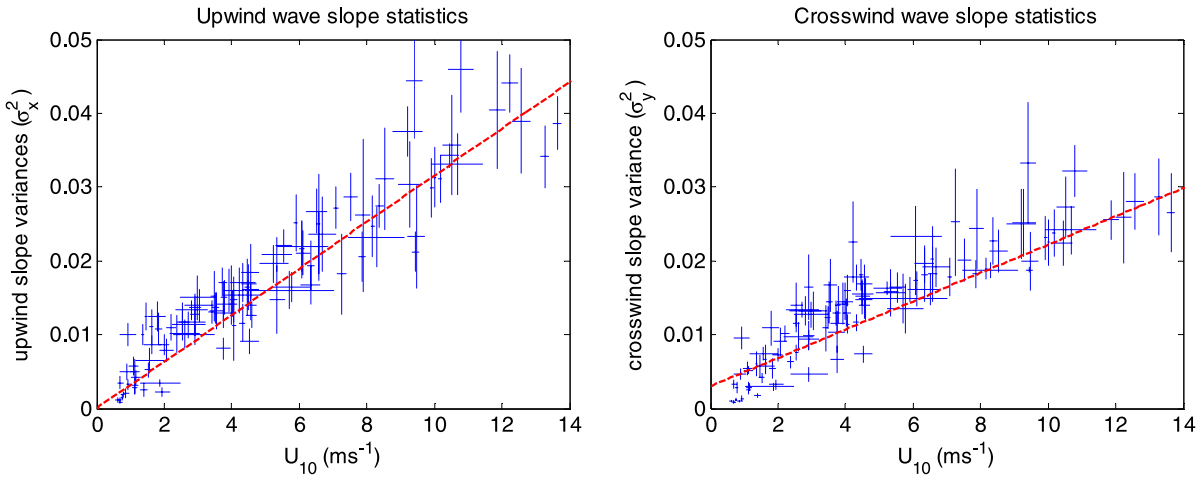

Figure 2. Sea surface slope variance correlation with wind speed at 10 m (U_{10}) in the (left) upwind and (right) crosswind resulting from the analysis of the COVE data. The dashed lines are the *Cox and Munk* [1954a, 1954b] models.

[18] In order to study the potential geometrical dependence on surface statistics, the same procedure is applied by binning the data in both wind speed and elevation angle increments. Because of the much reduced number of data points in each bin, the fitting error is much larger, so only the central moments method is used (because of possible convergence problems in the least squares algorithm) and the fitted variances are averaged back into larger wind speed bins. This is done because large wind speed intervals cannot be used to bin the PDF values as they tend to introduce a bias in the elevation dependence [*Ross and Dion*, 2004].

4. Results and Discussion

4.1. Sea Slope–Wind Speed Correlation

[19] The outcome of the statistical analysis of the data against wind speed at 10 meters is plotted in Figure 2. The ordinate error bars correspond to the least squares Gram-Charlier fit error while the abscissa errors are the standard deviations of the wind speed within the bin. Also plotted is the *Cox and Munk* [1954a, 1954b] slope variance model in the upwind and crosswind directions (dashed line). Like most other studies, our slope variance data follow the general trend established by *Cox and Munk* [1954a, 1954b], however the large number of data points presented here may let us extract finer trends in the wind-slope correlation. In fact, one can note a logarithmic trend in the data, especially in the crosswind direction and in the lower wind speed regime of the upwind variance data. This type of trend is often the result of the integration of wave spectra. Even older spectra that do not include a valid small gravity to capillary wave region such as the classic *Phillips* [1958] spectrum produce a similar trend, strengthening the hypothesis by *Wu* [1990] that small gravity and capillary waves are more significant at higher wind speeds. Because of the large uncertainties on our PDF data points, correlations of skewness and kurtosis with wind speed are not investigated here.

[20] The average of the upwind and crosswind variances resulting from the *Elfouhaily et al.* [1997] spectrum in a neutral atmosphere for a fully developed sea is plotted (solid line) against the data (crosses) in Figure 3. Error bars have been removed for clarity. Also plotted are the results of integrating the *Elfouhaily et al.* [1997] spectrum in strongly stable conditions (lower dashed line) and strongly unstable conditions (upper dashed line). The stable case has an air-sea temperature difference (ASTD) of +8°C while the unstable case has an ASTD of −8°C. In both cases, the sea temperature is 12°C. Even though the model trend is quite close to that of the data, especially at low wind speeds where the logarithmic tendency is well matched, the model seems to globally underestimate the data to a slight degree. It is worth noting that the study by *Shaw and Churnside* [1997] showed that under unstable to neutral conditions, measured variance ratios could reach factors close to 2.0, while the variances stemming from the *Elfouhaily et al.* [1997] spectrum, whose stability dependence stems from the wind friction speed (u_*), shows much smaller ratios.

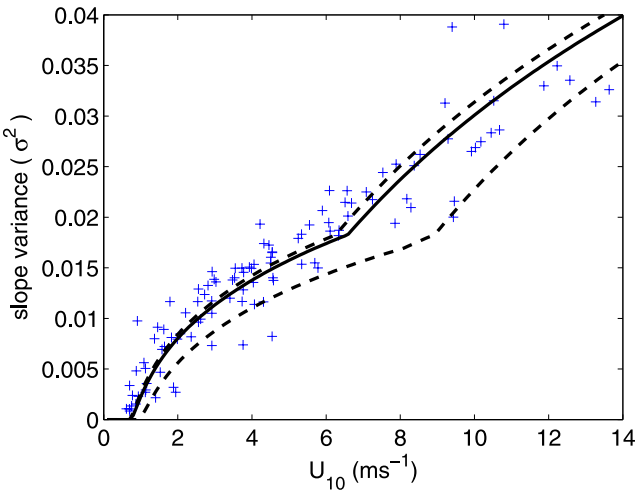

Figure 3. Average of the upwind and crosswind variance data plotted against variances obtained from the *Elfouhaily et al.* [1997] spectrum for a fully developed sea in neutral atmospheric conditions (solid line), stable conditions (lower dashed line), and unstable conditions (upper dashed line).

Table 1. Weighted Standard Deviation Between Our Slope Variance Data (Upwind and Crosswind Averaged) and Models From *Cox and Munk* [1954a, 1954b] and *Elfouhaily et al.* [1997] (Neutral Conditions, Fully Developed Sea) for $U_{10} < 7$ m s^{-1} (σ_{7-}), $U_{10} \geq 7$ m s^{-1} (σ_{7+}) and for the Entire Wind Speed Range (σ)

	Cox and Munk [1954a, 1954b]	*Elfouhaily et al.* [1997]
σ_{7-}	3.411E-03	2.699E-03
σ_{7+}	4.143E-03	4.408E-03
σ	3.696E-03	3.461E-03

Had the ratio been higher, the model would have encompassed much more of the data. Nevertheless, in Table 1 the *Elfouhaily et al.* [1997] model in neutral conditions and for a fully developed sea performs marginally better than the *Cox and Munk* [1954a, 1954b] model when compared to our data for the full extent of wind speeds. At low wind speeds, the gain in accuracy of the *Elfouhaily et al.* [1997] model is increased because it better reproduces the logarithmic trend discernable in the data.

[21] *Cox and Munk* [1954a, 1954b] indicate that upwind to crosswind slope variance ratios for clean water surfaces are higher on average than those for surfaces with natural or artificial slicks where waves shorter than 30 cm are suppressed. This seems to indicate that the ratio depends to some extent on the presence of small waves. In the gravity-capillary wave spectrum of *Elfouhaily et al.* [1997], the importance of small waves increases with wind speed. It could then be expected that the anisotropy between upwind and crosswind variances would also increase with wind speed. However, in the *Cox and Munk* [1954a, 1954b] measurements, this is not clear, with a nearly constant ratio σ_x^2/σ_y^2 of 1.34, showing what might be only a small increase at high wind speeds. In Figure 4, the σ_x^2/σ_y^2 ratio for our data is combined with that of *Cox and Munk* [1954a, 1954b] and is plotted against wind speed at 10 m. A weighted linear fit to our data is obtained in log space so that a particular ratio has equal weight to its inverse. The result (solid line) is the exponential relation

$$\sigma_x^2/\sigma_y^2 = \exp(0.0275U_{10} + 0.0143) \tag{17}$$

which increases from nearly unity at low wind speeds to about 1.5 at 14 m s^{-1}. Also plotted in Figure 4 is the σ_x^2/σ_y^2 ratio for the *Elfouhaily et al.* [1997] model in a neutral atmosphere (dashed line), which decreases with wind speed. This unexpected result is due to the angular spreading function term, $\Delta(k)$ in equation (1), which might not favor anisotropy in the small wave domain sufficiently. (For convenience, a summary of the slope data used in this paper is presented in Table 2.)

4.2. Atmospheric Stability

[22] Although sea surface temperature measurements at the COVE site were not available for the period at which radiance measurements were made, they can be deduced by extrapolation from neighboring National Oceanic and Atmospheric Administration (NOAA) platform and buoy measurements. Because of the resulting uncertainties of surface temperatures, and as a consequence of the noisy nature of the data, a fine analysis of the correlation between slope variances and atmospheric stability could not be performed with the accuracy of other studies. However, the extent of the data shows an interesting trend in the very stable or very unstable domains. Figure 5 plots the ratio of our slope variance to the *Cox and Munk* [1954a, 1954b] model as a function of the Monin-Obukhov parameter z/L, where L is known as the length scale. Not much can be said other than the fact that σ^2/σ_{cm}^2 seems to level off at roughly 0.5 in stable atmospheres (positive values of z/L) and to fall back under 1.5 in very unstable cases (negative values). The stable case is in agreement with the observations of *Hwang*

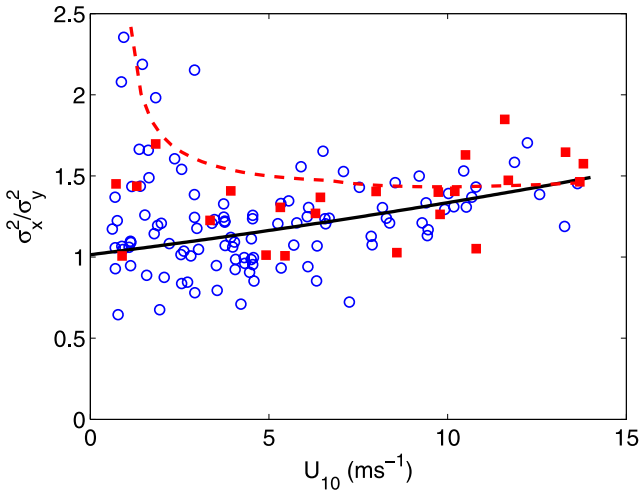

Figure 4. Ratio of upwind to crosswind slope variance for this study's data (circles) and for the *Cox and Munk* [1954a, 1954b] data (squares) plotted against wind speed at 10 m. The solid line is the fitted trend to this study's data and the dashed line is the result from the *Elfouhaily et al.* [1997] model for a neutral atmosphere.

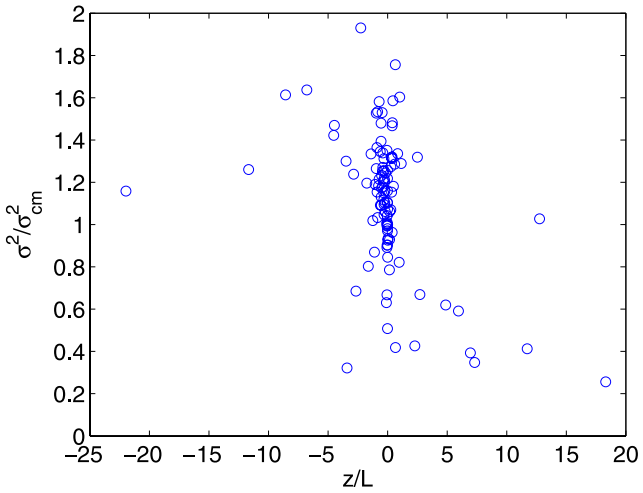

Figure 5. Ratio of our slope variances and those of *Cox and Munk* [1954a, 1954b] against z/L to show dependence with atmospheric stability. One outlier point is not shown to constrain the scale of the axes.

Table 2. Data Summary

Date (dd-mm-yyyy)	U_{10}, m s^{-1a}	ΔU_{10}, m s^{-1}	σ_x	$\Delta\sigma_x$	σ_y	$\Delta\sigma_y$	z/L^b
30-08-2003	4.066	0.044	1.131e-2	4.747e-3	1.147e-2	1.278e-3	0.384
30-08-2003	4.309	0.087	1.161e-2	2.515e-3	1.164e-2	1.124e-3	0.037
30-08-2003	5.778	0.546	1.641e-2	1.968e-3	1.355e-2	3.412e-3	0.014
04-09-2003	3.475	0.08	1.522e-2	3.370e-3	1.237e-2	1.514e-3	0.840
04-09-2003	3.986	0.25	1.539e-2	3.997e-3	1.450e-2	2.562e-3	0.583
25-09-2003	2.211	0.134	1.096e-2	1.755e-3	1.012e-2	1.099e-3	0.393
04-09-2003	2.537	0.089	1.175e-2	1.641e-3	1.157e-2	1.232e-3	0.383
04-09-2003	2.914	0.181	1.362e-2	1.570e-3	9.834e-3	2.015e-3	0.315
04-09-2003	3.736	0.255	1.294e-2	9.720e-4	1.039e-2	2.770e-3	0.177
26-09-2003	0.699	0.079	3.460e-3	8.380e-4	3.271e-3	6.630e-4	12.755
26-09-2003	1.086	0.132	5.780e-3	1.194e-3	5.454e-3	8.880e-4	2.496
26-09-2003	1.37	0.038	9.974e-3	1.395e-3	5.994e-3	1.711e-3	1.010
26-09-2003	1.456	0.036	1.253e-2	1.844e-3	5.728e-3	1.560e-3	0.643
26-09-2003	1.621	0.045	1.111e-2	2.339e-3	6.703e-3	1.889e-3	0.441
26-09-2003	1.83	0.089	1.079e-2	2.173e-3	5.443e-3	1.369e-3	0.374
27-09-2003	3.407	0.085	1.312e-2	1.532e-3	1.087e-2	3.110e-3	0.485
27-09-2003	3.775	0.084	1.505e-2	2.305e-3	1.405e-2	2.508e-3	0.362
27-09-2003	4.037	0.108	1.415e-2	1.756e-3	1.296e-2	1.915e-3	0.338
27-09-2003	4.566	0.165	1.400e-2	2.056e-3	1.404e-2	1.865e-3	0.265
03-10-2003	1.128	0.128	4.917e-3	1.676e-3	5.195e-3	4.760e-4	−21.978
03-10-2003	1.576	0.428	6.522e-3	1.689e-3	7.349e-3	9.110e-4	−11.669
13-10-2003	3.029	0.427	1.392e-2	2.227e-3	1.329e-2	2.615e-3	−0.551
15-10-2003	10.792	0.378	4.600e-2	5.857e-3	3.214e-2	3.531e-3	−0.055
15-10-2003	11.873	0.238	4.044e-2	8.006e-3	2.554e-2	2.674e-3	−0.038
15-10-2003	12.574	0.271	3.897e-2	7.089e-3	2.811e-2	3.804e-3	−0.045
15-10-2003	13.272	0.121	3.411e-2	4.215e-3	2.869e-2	5.193e-3	−0.052
15-10-2003	13.634	0.125	3.863e-2	3.576e-3	2.659e-2	5.342e-3	−0.046
16-10-2003	3.73	0.113	1.708e-2	1.897e-3	1.287e-2	1.701e-3	−0.903
16-10-2003	4.217	0.126	1.603e-2	3.057e-3	2.259e-2	5.543e-3	−0.715
16-10-2003	4.458	0.076	1.640e-2	3.840e-3	1.810e-2	2.197e-3	−0.616
16-10-2003	5.335	0.438	2.091e-2	2.279e-3	1.572e-2	3.238e-3	−0.303
16-10-2003	6.349	0.092	1.933e-2	3.417e-3	1.809e-2	3.593e-3	−0.206
16-10-2003	6.567	0.042	2.500e-2	6.771e-3	2.023e-2	4.497e-3	−0.169
19-10-2003	2.814	0.47	1.331e-2	1.308e-3	1.322e-2	1.938e-3	−0.839
19-10-2003	4.323	0.375	1.706e-2	2.560e-3	1.774e-2	1.831e-3	−0.558
24-10-2003	2.722	0.491	1.133e-2	1.700e-3	1.340e-2	1.098e-3	−4.474
24-10-2003	4.503	0.311	1.536e-2	1.994e-3	1.559e-2	1.649e-3	−1.752
24-10-2003	5.342	0.223	1.481e-2	4.595e-3	1.589e-2	1.195e-3	−1.244
24-10-2003	6.334	0.289	1.673e-2	2.599e-3	1.962e-2	2.537e-3	−0.839
24-10-2003	7.25	0.146	1.823e-2	5.395e-3	2.524e-2	7.252e-3	−0.614
24-10-2003	7.887	0.219	2.616e-2	1.028e-2	2.433e-2	5.452e-3	−0.505
30-10-2003	0.695	0.024	1.214e-3	2.140e-4	8.870e-4	1.650e-4	−3.407
30-10-2003	0.778	0.048	1.869e-3	3.230e-4	2.896e-3	7.720e-4	−2.661
30-10-2003	1.161	0.127	4.211e-3	9.450e-4	2.934e-3	5.080e-4	−1.628
30-10-2003	1.525	0.083	5.207e-3	1.052e-3	4.135e-3	6.960e-4	−1.104
30-10-2003	1.987	0.144	8.707e-3	1.372e-3	7.204e-3	9.230e-4	−0.714
30-10-2003	2.36	0.098	1.008e-2	2.542e-3	6.279e-3	8.770e-4	−0.528
30-10-2003	2.557	0.04	1.168e-2	1.204e-3	7.580e-3	1.082e-3	−0.373
02-11-2003	0.616	0.049	1.150e-3	2.440e-4	9.810e-4	1.980e-4	7.310
02-11-2003	0.755	0.035	1.478e-3	3.880e-4	1.208e-3	2.640e-4	6.944
02-11-2003	0.936	0.043	3.216e-3	7.490e-4	1.366e-3	3.680e-4	5.942
02-11-2003	1.136	0.091	3.061e-3	1.135e-3	2.808e-3	7.280e-4	2.704
02-11-2003	1.642	0.248	8.640e-3	1.221e-3	5.804e-3	1.187e-3	0.261
03-11-2003	0.702	0.054	8.090e-4	1.560e-4	8.720e-4	1.990e-4	18.315
03-11-2003	0.869	0.086	2.066e-3	6.460e-4	9.940e-4	1.870e-4	11.723
03-11-2003	1.125	0.069	2.825e-3	7.050e-4	2.574e-3	6.050e-4	4.876
03-11-2003	1.4	0.089	2.541e-3	8.680e-4	1.768e-3	3.680e-4	2.281
03-11-2003	1.943	0.225	2.172e-3	5.970e-4	3.215e-3	6.290e-4	0.660
03-11-2003	2.919	0.549	9.996e-3	1.380e-3	4.644e-3	9.940e-4	0.972
25-12-2003	6.109	0.207	2.110e-2	3.010e-3	1.617e-2	2.375e-3	−0.298
25-12-2003	6.587	0.128	2.198e-2	4.619e-3	1.824e-2	3.758e-3	−0.243
26-12-2003	4.547	0.239	1.612e-2	1.007e-3	1.690e-2	2.530e-3	−0.958
26-12-2003	5.551	0.237	2.207e-2	2.233e-3	1.639e-2	2.027e-3	−0.508
26-12-2003	5.897	0.052	2.515e-2	3.891e-3	1.615e-2	1.645e-3	−0.435
26-12-2003	6.071	0.059	2.162e-2	3.893e-3	1.732e-2	1.983e-3	−0.335
26-12-2003	6.686	0.4	2.369e-2	5.049e-3	1.911e-2	2.669e-3	−0.241
27-12-2003	9.287	0.36	3.039e-2	5.797e-3	2.511e-2	4.593e-3	−0.017
27-12-2003	9.92	0.057	2.989e-2	3.942e-3	2.311e-2	2.987e-3	−0.041
27-12-2003	10.025	0.032	3.128e-2	4.054e-3	2.248e-2	3.102e-3	−0.037
27-12-2003	10.173	0.045	3.115e-2	3.208e-3	2.379e-2	3.179e-3	−0.051
27-12-2003	10.45	0.271	3.429e-2	1.619e-3	2.241e-2	3.003e-3	−0.049
28-12-2003	2.07	0.194	7.913e-3	1.535e-3	9.042e-3	1.871e-3	−0.296

Table 2. (continued)

Date (dd-mm-yyyy)	U_{10}, m s^{-1a}	ΔU_{10}, m s^{-1}	σ_x	$\Delta\sigma_x$	σ_y	$\Delta\sigma_y$	z/L^b
28-12-2003	2.919	0.306	1.165e-2	1.799e-3	9.363e-3	1.337e-3	−0.423
28-12-2003	3.53	0.1	1.364e-2	2.099e-3	1.439e-2	2.784e-3	−0.402
28-12-2003	3.93	0.173	1.592e-2	2.912e-3	1.421e-2	2.773e-3	−0.313
28-12-2003	4.581	0.151	1.265e-2	1.787e-3	1.485e-2	2.830e-3	−0.296
30-12-2003	8.286	0.82	2.320e-2	4.030e-3	1.871e-2	1.013e-3	0.165
30-12-2003	9.431	0.101	2.125e-2	2.635e-3	1.877e-2	4.180e-4	0.147
31-12-2003	0.911	0.235	9.971e-3	1.542e-3	9.528e-3	1.493e-3	−4.924
31-12-2003	1.787	0.242	1.244e-2	1.991e-3	1.088e-2	2.361e-3	−2.260
31-12-2003	2.983	0.517	1.499e-2	3.002e-3	1.273e-2	1.777e-3	−0.960
31-12-2003	4.545	0.244	1.847e-2	3.801e-3	1.468e-2	1.055e-3	−0.407
31-12-2003	5.249	0.415	1.958e-2	2.472e-3	1.624e-2	9.160e-4	−0.258
01-01-2004	0.88	0.187	4.970e-3	1.054e-3	4.661e-3	8.320e-4	1.138
01-01-2004	1.883	0.579	3.476e-3	4.810e-4	2.910e-3	5.630e-4	−0.009
01-01-2004	3.762	0.204	8.119e-3	1.452e-3	6.648e-3	1.769e-3	−0.054
01-01-2004	4.542	0.268	9.088e-3	1.668e-3	7.354e-3	1.114e-3	−0.099
07-01-2004	6.512	0.289	2.675e-2	2.929e-3	1.619e-2	2.151e-3	−1.050
07-01-2004	7.084	0.055	2.719e-2	2.823e-3	1.781e-2	2.634e-3	−0.887
07-01-2004	7.53	0.204	2.873e-2	3.221e-3	2.009e-2	2.891e-3	−0.764
07-01-2004	8.534	0.261	3.109e-2	6.914e-3	2.132e-2	2.955e-3	−0.542
07-01-2004	9.397	0.236	4.437e-2	7.817e-3	3.325e-2	8.213e-3	−0.465
07-01-2004	10.522	0.267	3.572e-2	6.720e-3	2.732e-2	4.157e-3	−0.322
11-01-2004	2.556	0.175	1.175e-2	2.565e-3	1.404e-2	2.981e-3	−8.576
11-01-2004	2.925	0.137	1.281e-2	2.757e-3	1.642e-2	4.463e-3	−6.784
11-01-2004	3.551	0.202	1.324e-2	2.445e-3	1.667e-2	3.545e-3	−4.531
11-01-2004	4.055	0.104	1.472e-2	3.088e-3	1.595e-2	2.140e-3	−3.497
11-01-2004	4.509	0.209	1.689e-2	2.659e-3	1.519e-2	2.365e-3	−2.860
11-01-2004	6.089	0.766	2.195e-2	3.358e-3	2.332e-2	4.182e-3	−1.394
18-02-2004	10.677	0.761	3.308e-2	4.148e-3	2.417e-2	3.274e-3	−0.004
18-02-2004	12.231	0.223	4.406e-2	3.870e-3	2.586e-2	6.228e-3	−0.002
22-02-2004	2.617	0.437	1.010e-2	1.929e-3	9.747e-3	2.002e-3	−0.008
22-02-2004	3.764	0.21	1.407e-2	3.076e-3	1.158e-2	1.244e-3	−0.008
22-02-2004	5.694	1.314	1.603e-2	2.508e-3	1.493e-2	3.326e-3	−0.006
22-02-2004	9.457	0.266	2.325e-2	6.937e-3	1.990e-2	3.981e-3	−0.003
25-02-2004	7.86	0.11	2.055e-2	3.371e-3	1.823e-2	1.881e-3	−0.014
25-02-2004	8.175	0.042	2.471e-2	4.153e-3	1.894e-2	1.466e-3	−0.012
25-02-2004	8.374	0.112	2.749e-2	2.929e-3	2.272e-2	3.227e-3	−0.011
25-02-2004	9.205	0.439	3.752e-2	3.413e-3	2.503e-2	4.760e-3	−0.006

[a]Scaled to 10 m from 38 m using the Monin-Obukhov theory.
[b]Estimated from the Monin-Obukhov theory and extrapolated sea surface temperature.

and Shemdin [1988], whose data leveled at about 0.6 in stable cases.

4.3. Grazing Elevation Angles

[23] Most sea surface BRDF models that rely on statistical optics make the approximation that there is no correlation between the probability that a given slope will occur on a small surface area and the height of that surface area above the mean sea surface height. This hypothesis is in fact fundamental in the derivation of equation (12). Studies such as those from *Bourlier et al.* [2000a, 2000b] have suggested that this approximation may in fact lead to errors. These errors, however, are difficult to evaluate experimentally since they are likely to occur in peculiar source-viewing geometries. With the detailed BRDF used in this analysis, the effect on slope variance measurements for viewing angles close to the horizon when the viewing geometry favors more elevated wave surfaces should become apparent. Since the BRDF already incorporates first-order shadowing and hiding of waves using the *Smith* [1967a, 1967b] function, as shadowing becomes more important, any deviations in measured slope variance values should essentially be a manifestation of the error made by not considering the height-slope correlation. Measurements of this effect can be used to minimize the error empirically as discussed below.

[24] The result of the statistical analysis done by binning the data in elevation is shown in Figure 6 (circles) where the slope variances are plotted as a function of surface to sensor elevation. Elevation values are corrected for earth curvature and atmospheric refraction, although this correction is usually minor. Results for high wind speeds (>6 m s^{-1}) and low wind speeds (<6 m s^{-1}) are plotted separately to verify wind speed dependence.

[25] It is clear from Figure 6 that there exists a correlation between elevation angle and measured slope variance, with higher variances values near the horizon, and that the correlation holds for high and low wind speeds. Near the horizon the receiver mostly detects reflections off the very tops of waves, the vast majority of troughs being hidden from view by other waves (Figure 7). This means that slopes tend to be steeper when the wave facets are located higher above the mean surface level, which in turn implies a notable slope-height correlation. In agreement with this interpretation, many authors such as *Longuet-Higgins* [1963], *Phillips* [1977], and *Liu et al.* [1997, 2000] contend that the departure of the sea slope PDF from Gaussian might

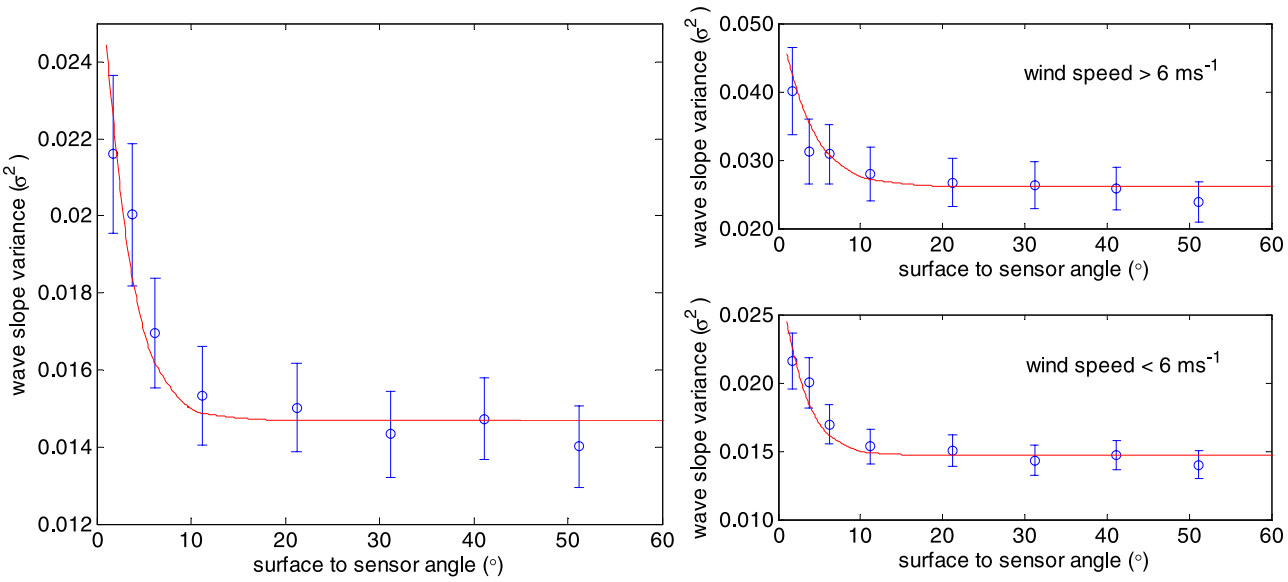

Figure 6. Surface to detector elevation angle dependence of slope variances.

be the consequence of sharp crests and shallow troughs. Another, but not completely unrelated explanation is that there might be an accrued presence of short waves generated or amplified at the crests of larger gravity waves, such as those described by investigators such as *Cox* [1958], *Perlin et al.* [1993], *Longuet-Higgins* [1963, 1992, 1995], and *Hwang* [2001]. It is plausible that these small waves play a role in the increased measured slope variance at grazing angles.

[26] Although the analytical sea BRDF model introduced by *Ross et al.* [2005] (equations (11)–(15)) is based on an uncorrelated near Gaussian surface, it may still be possible to incorporate some of the effects of height-slope correlation with a few approximations. The key is to realize that, from a geometrical optics perspective, the statistics of the surface regions that the receiver cannot detect (the troughs, for example) have little impact on the measured radiance apart from second-order contributions like multiple reflections and shadowing. We can thus introduce the concept of effective variance, defined by the average variance of the portion of the surface that is visible from the detector. We can approximate this concept mathematically by using the integrated uncorrelated *Smith* [1967a, 1967b] shadowing function H_w on a Gaussian height distribution $p(h)$ of variance σ_h

$$\begin{aligned} f_s(\boldsymbol{\Psi}_r, \sigma(\phi)) &= \int_{-\infty}^{\infty} p(h) H_w(h, \boldsymbol{\Psi}_r) dh \\ &= \frac{1}{\sigma_h \sqrt{2\pi}} \int_{-\infty}^{\infty} \exp\left(\frac{h^2}{2\sigma_h^2}\right) \\ &\quad \times \left[1 - \frac{1}{2}\mathrm{erfc}(h)\right]^{\Lambda(v_r)} dh \\ &= \frac{1}{1 + \Lambda(v_r)}, \end{aligned} \tag{18}$$

where f_s represents the fraction of the surface visible in a given viewing geometry. The use of the uncorrelated shadowing function is justified since it introduces errors smaller than 4% on f_s when compared to the much more complex correlated shadowing function [*Bourlier et al.*, 2000a]. If we make the assumption that slope variances vary linearly from trough to crest, and that all surface elements located in the lower $1 - f_s$ fraction of surface heights are hidden from view, the effective variance can be given by

$$\sigma_{eff}^2 = \gamma(1 - f_s)\overline{\sigma}^2 + f_s\overline{\sigma}^2 \tag{19}$$

where $\overline{\sigma}^2$ is the average variance of the entire surface (including troughs) as given by most variance models, and

$$\gamma = \frac{\sigma_c^2}{\overline{\sigma}^2} \tag{20}$$

with σ_c^2 being the wave crest slope variance. The resulting model using γ = 1.5 and with $\overline{\sigma}^2$ calculated by averaging data points with surface to receiver elevation higher than 20° is plotted in Figure 6, and is a good fit to the observed trend. The *Cox and Munk* [1954a, 1954b] or *Elfouhaily et al.* [1997] model could have been used for $\overline{\sigma}^2$, but the intent was to investigate the trend near the horizon, not to validate these models. Also note that $\overline{\sigma}^2$ should be used instead of σ_{eff}^2 in equation (15) and in the calculation of f_s (the relation is not recursive). This is because the statistics of the entire surface as a whole, not only of the visible part, are responsible for the shadowing of troughs.

[27] Another interpretation of the apparent increase in variance might include multiple reflections. It has been estimated by *Preisendorfer and Mobley* [1986] and *Henderson et al.* [2003] that 10 to 15% of the rays that arrive at a detector have been reflected more than once. Since the average reflectance (albedo) of water is never much greater than 20% [*Jin et al.*, 2002], the error should

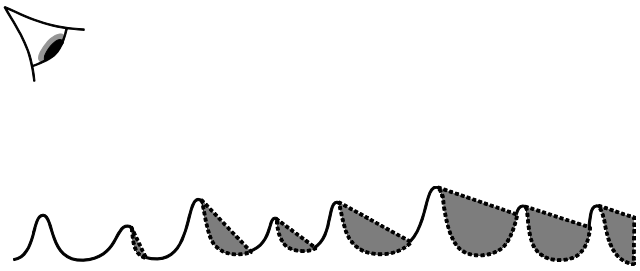

Figure 7. Hiding of wave troughs by shadowing at grazing angles.

not exceed 2 to 3% with the largest errors occurring at high wind speeds, low Sun elevations and near horizontal detector orientations. Although the effects of multiple reflections also occur mainly near the horizon, it is unlikely to have enough amplitude to produce the observed effect, so the first explanation seems more probable. Also, there does not seem to be much correlation with wind speed as there should be if the effect was caused by multiple reflections reinforcing the shadowing origin to the trend. In any case, if multiple reflections play a small part, their effect will be included to some extent in the empirical value of γ, thus adding their effect in the resulting BRDF.

[28] Because no data was analyzed with the Sun elevation lower than 10°, a similar analysis could not be done with solar geometry, but if the hypotheses leading to expression (19) are correct, the combined Sun shadowing and receiver hiding expression should be used for modeling reflections of low source elevations

$$f_s = \frac{1}{1 + \Lambda(v_r) + \Lambda(v_s)} \tag{21}$$

5. Conclusion

[29] Since accuracy of sea slope variances directly affect the precision of most reflectivity calculations, increasing the exactness of variance models is critical. In this study, sea surface solar glint radiance measurements were used to derive surface slope variance values. In order to do so, an advanced analytical BRDF that includes first-order wave mutual shadowing and hiding, and wave facet weighing was inverted to obtain values of slope PDF, to which a Gram-Charlier distribution function was fitted with the upwind and crosswind slope variances as free parameters. The resulting slope variances were correlated with wind speed and yielded trends very similar to those of other studies of the likes of *Cox and Munk* [1954a, 1954b] and *Elfouhaily et al.* [1997]. In particular, the integration of the *Elfouhaily et al.* [1997] spectrum into slope variances produces some of the finer trends visible in the data, although wind direction and stability dependence of the modeled slope variances still fail to agree with this and other earlier studies. Because of uncertainties on sea surface temperatures, correlation of the variances with atmospheric stability could not be thoroughly investigated. However, our analysis suggests that the ratio of measured variances to those of *Cox and Munk* [1954a, 1954b] level off to about 0.5 at high stability as noted in other studies and fall back to a value under 1.5 at high instability.

[30] Since a first-order shadowing is included in the BRDF, it was possible to analyze measurements against the surface to receiver angle with some added accuracy. A strong increase in slope variances was noted toward near horizontal viewing angles, suggesting a slope-height correlation. The notion of effective slope variances was introduced in order to empirically add the second-order effect of shadowing, one that affects the perceived statistics of the surface being viewed, to statistical BRDF models. Although approximate, this manner of introducing height-slope correlation should improve the accuracy of radiance models when the receiver or source is at a grazing angle.

[31] The simplicity of the method used here to obtain slope variances implies that any high dynamic range imaging of solar glint can be used to expand our knowledge of sea surface statistics and eventually even improve upon existing wave spectra models.

[32] **Acknowledgments.** The authors give many thanks to Ken Rutledge for providing precious information about the data used in this study. Thanks also to David Rutan for promptly making available to us the meteorological data from the CERES Ocean Validation Experiment (COVE) site. Funds for this research have been provided by the Department of National Defense of Canada.

References

Acharya, P. K., A. Berk, G. P. Anderson, N. F. Larsen, S.-C. Tsay, and K. H. Stamnes (1999), MODTRAN4: Multiple scattering and bi-directional reflectance distribution function (BRDF) upgrades to MODTRAN, in *Optical Spectroscopy Techniques and Instrumentation for Atmospheric and Space Research III*, vol. 3756, pp. 19–21, SPIE Int. Soc. for Opt. Eng., Bellingham, Wash.

Apel, J. R. (1994), An improved model of the ocean surface wave vector spectrum and its effects on radar backscatter, *J. Geophys. Res.*, *99*, 16,269–16,291.

Berk, A., L. S. Bernstein, and D. C. Robertson (1989), MODTRAN: A moderate resolution model for LOWTRAN7, *Tech. Rep. GL-TR-89-0122*, Air Force Geophys. Lab., Bedford, Mass.

Bourlier, C., J. Saillard, and G. Berginc (2000a), Effect of correlation between shadowing and shadowed points on the Wagner and Smith monostatic one-dimensional shadowing function, *IEEE Trans. Anttennas Propag.*, *48*, 437–446.

Bourlier, C., J. Saillard, and G. Berginc (2000b), Effect of the observation length on the two-dimentional shadowing function of the sea surface: Application on infrared 3-13-μm emissivity, *Appl. Opt.*, *39*, 3433–3442.

Cox, C. (1958), Measurement of slopes of high-frequency wind waves, *J. Mar. Res.*, *16*, 199–225.

Cox, C., and W. Munk (1954a), Measurement of the roughness of the sea surface from photographs of the Sun glitter, *J. Opt. Soc. Am.*, *44*, 838–850.

Cox, C., and W. Munk (1954b), Statistics of the sea surface derived from Sun glitter, *J. Mar. Res.*, *13*, 198–227.

Dion, D., L. Gardenal, J. L. Forand, M. Duffy, G. Potvin, and S. Daigle (2004), *IR Boundary Layer Effects Model (IRBLEM): IRBLEM5.1 Documentation*, Def. Res. and Dev. Can., Valcartier, Que.

Donelan, M. A., and W. J. Pierson (1987), Radar scattering and equilibrium range in wind-generated waves with application to scatterometry, *J. Geophys. Res.*, *92*, 4971–5029.

Elfouhaily, T., B. Chapron, K. Katsaros, and D. Vandemark (1997), A unified directional spectrum for long and short wind-driven waves, *J. Geophys. Res.*, *102*, 15,781–15,796.

Forand, J. L. (1999), The L(W)WKD marine boundary layer model—Version 7.09, *Tech. Rep. 1999-099*, Def. Res. Estab. of Valcartier, Valcartier, Queb., Canada.

Haimbach, S. P., and J. Wu (1985), Field trials of an optical scanner for studying sea-surface fine structures, *IEEE J. Oceanic Eng.*, *OE-10*, 451–453.

Hara, T., E. J. Bock, and D. Lyzenga (1994), In situ measurements of capillary-gravity wave spectra using a scanning laser slope gauge and microwave radars, *J. Geophys. Res.*, *99*, 12,593–12,602.

Hasselmann, K., et al. (1973), Measurements of wind-wave growth and swell decay during the Joint North Sea Wave Project (JONSWAP), *Dtsch. Hydrogr. Z.*, *8*, 95 pp., suppl. A.

Henderson, B., J. Theiler, and P. V. Villeneuve (2003), The polarized emissivity of a wind-roughened sea surface: A Monte-Carlo model, *Remote Sens. Environ.*, *88*, 453–467.

Hughes, B. A., H. L. Grant, and R. W. Chappell (1977), A fast response surface-wave slope meter and measured wind-wave moments, *Deep Sea Res.*, *24*, 1211–1223.

Hwang, P. A. (2001), Phase distribution of small-scale ocean surface roughness, *J. Phys. Oceanogr.*, *32*, 2977–2987.

Hwang, P. A. (2005), Wave number spectrum and mean square slope of intermediate-scale ocean surface waves, *J. Geophys. Res.*, *110*, C10029, doi:10.1029/2005JC003002.

Hwang, P. A., and O. H. Shemdin (1988), The dependence of sea surface slope on atmospheric stability and swell conditions, *J. Geophys. Res.*, *93*, 13,903–13,912.

Jähne, B., and K. S. Riemer (1990), Two-dimensional wave number spectra of small-scale water surface waves, *J. Geophys. Res.*, *95*, 11,531–11,546.

Jin, Z., T. Charlock, and K. Rutledge (2002), Analysis of broadband solar radiation and albedo over the ocean surface at COVE, *Am. Meteorol. Soc.*, *19*, 1585–1601.

Liu, Y., X.-H. Yan, and P. A. Hwang (1997), The probability density function of the ocean surface slopes and its effects on radar backscatter, *J. Phys. Oceanogr.*, *27*, 782–797.

Liu, Y., M.-Y. Su, X.-H. Yan, and W. T. Liu (2000), The mean-square slope of ocean surface waves and its effects on radar backscatter, *J. Atmos. Oceanic Technol.*, *17*, 1092–1105.

Longuet-Higgins, M. S. (1963), The generation of capillary gravity waves by steep gravity waves, *J. Fluid Mech.*, *16*, 138–159.

Longuet-Higgins, M. S. (1992), Capillary rollers and bores, *J. Fluid Mech.*, *240*, 659–679.

Longuet-Higgins, M. S. (1995), Parasitic capillary waves: A direct calculation, *J. Fluid Mech.*, *301*, 79–107.

Mermelstein, M., E. Shettle, E. Takken, and R. Priest (1994), Infrared radiance and solar glint at the ocean-sky horizon, *Appl. Opt.*, *33*, 6022–6034.

Monin, A. S., and A. M. Obukhov (1954), Basic laws of turbulent mixing in the atmosphere near the ground, *Tr. Akad. Nauk SSSR Geofiz. Inst.*, *24*, 163–187.

Perlin, M., H. Lin, and C.-L. Ting (1993), On parasitic capillary waves generated by steep gravity waves: An experimental investigation with spatial and temporal measurements, *J. Fluid Mech.*, *255*, 597–620.

Phillips, O. M. (1958), The equilibrium range in the spectrum of wind-generated waves, *J. Fluid Mech.*, *4*, 426–434.

Phillips, O. M. (1977), *The Dynamics of the Upper Ocean*, 2nd ed., 336 pp., Cambridge Univ. Press, New York.

Phillips, O. M. (1985), Spectral and statistical properties of the equilibrium range in wind-generated gravity waves, *J. Fluid Mech.*, *156*, 505–531.

Plant, W. J. (2003), A new interpretation of sea-surface slope probability density functions, *J. Geophys. Res.*, *108*(C9), 3295, doi:10.1029/2003JC001870.

Preisendorfer, R. W., and C. D. Mobley (1986), Albedos and glitter patterns of a wind-roughened sea surface, *J. Phys. Oceanogr.*, *16*, 1293–1316.

Ross, V., and D. Dion (2004), Assessment of sea slope statistical models using a detailed micro-facet BRDF and upwelling radiance measurements, in *Optics in Atmospheric Propagation and Adaptive Systems VII*, vol. 5572, edited by J. D. Gonglewski and K. Stein, pp. 112–122, SPIE Int. Soc. for Opt. Eng., Bellingham, Wash.

Ross, V., D. Dion, and G. Potvin (2005), Detailed analytical approach to the Gaussian surface bidirectional reflectance distribution function specular component applied to the sea surface, *J. Opt. Soc. Am. A Opt. Image Sci.*, *22*, 2442–2453.

Rutan, D., F. Rose, N. Smith, and T. Charlock (2001), Validation data set for CERES Surface and Atmospheric Radiation Budget (SARB), *World Clim. Res. Programme Global Energy Water Cycle Exp. Newsl.*, *11*, 11–12.

Shaw, J. A., and J. H. Churnside (1997), Scanning-laser glint measurements of sea-surface slope statistics, *Appl. Opt.*, *36*, 4202–4213.

Shemdin, O. H., and P. A. Hwang (1988), Comparison of measured and predicted sea surface spectra of short waves, *J. Geophys. Res.*, *93*, 13,883–13,890.

Smith, B. G. (1967a), Lunar surface roughness, shadowing and thermal emission, *J. Geophys. Res.*, *72*, 4059–4067.

Smith, B. G. (1967b), Geometrical shadowing of a random rough surface, *IEEE Trans. Antennas Propag.*, *15*, 668–671.

Su, W., T. Charlock, and K. Rutledge (2002), Observations of reflectance distribution around sunglint from a coastal ocean platform, *Appl. Opt.*, *41*, 7369–7383.

Tang, S., and O. H. Shemdin (1983), Measurement of high-frequency waves using a wave follower, *J. Geophys. Res.*, *88*, 9832–9840.

Toba, Y. (1973), Local balance in the air-sea boundary processes, III, On the spectrum of wind waves, *J. Oceanogr. Soc. Jpn.*, *29*, 209–225.

Wu, J. (1972), Sea-surface slope and equilibrium wind-wave spectra, *Phys. Fluids*, *13*, 741–747.

Wu, J. (1990), Mean squared slopes of the wind-disturbed water surface, their magnitude, directionality, and composition, *Radio Sci.*, *25*, 37–48.

Zeisse, C. R. (1994), Radiance of the ocean horizon, *Tech. Rep. NCCOSC RDT&E TR-1660*, RDT&E Div., Nav. Command Control and Ocean Surveillance Cent., San Diego, Calif.

Zeisse, C. R. (1995), Radiance of the ocean horizon, *J. Opt. Soc. Am.*, *12*, 2022–2030.

D. Dion, Defence Research and Development Canada-Valcartier, 2459 Pie-XI Blvd. North, Quebec, QC, Canada G3J 1X5. (denis.dion@drdc-rddc.gc.ca)

V. Ross, AEREX Avionique Inc. 36 du Ruisseau, Suite 102, Breakeyville, QC, Canada G0S 1E2. (vross@aerex.ca)